Bull. Mar. Sci & Tech 1 0(1), 2001
Research Institute of Marine Science and Technology
Korea Maritime University

J. Acoust. Soc. Am.
109(5), 2001

Adaptive time-reversal mirror

J. S. Kim,[a] H. C. Song and W. A. Kuperman

Marine Physical Laboratory, Scripps Institute of Oceanography, University of California, San Diego, La Jolla, California 92093-0238

(Received 20 December 2000; revised 1 February 2001; accepted 2 February 2001)

The time-reversal mirror uses the received signal from a probe source to refocus the signal at the probe source location by backpropagating the time-reversed version of the received signal. In this study, an adaptive method is described to steer a null to an arbitrary position in a waveguide while maintaining a distortionless response at the probe source location. As an application, selective focusing in free space is demonstrated. © *2001 Acoustical Society of America.*
[DOI: 10.1121/1.1358299]

PACS numbers: 43.20.Fn, 43.30.Vh [ANN]

I. INTRODUCTION

The time-reversal mirror (TRM) has been demonstrated in ultrasonics[1,2] and underwater acoustic environments.[3] Further, the theory has been extended to the detection of scatterers and to focusing through an inhomogeneous medium. Recently, the development of the DORT method[4] allowed the selective focusing on a weak scatterer.

In this paper, the concept of an adaptive weighting on the TRM array before backpropagation is introduced to steer nulls. Accordingly, the expression for the weight vector to steer a null at the arbitrary location, assuming that the cross-spectral density matrix (CSDM) for the null location is known, is formulated based on optimization theory with constraints.[5-7] Then, it is demonstrated in simulation that the null can be steered in an ocean waveguide. Even when the CSDM is not available, a null in the vicinity of the probe source still can be steered in the range direction based on the theory on the invariants of the waveguide,[8-11] for which simulation results are also given.

As an application of null steering, selective focusing on the weaker target among two targets is demonstrated, and compared with the previous work known as the DORT method.[4,12] In order to focus on the strong target, the iterative time-reversal mirror[13-15] is used. It is shown that the focused field on the strong scatterer is equivalent to the field due to the eigenvector with the largest eigenvalue propagated to the control plane, where the scatterers are located. Since the scattered field from the strong scatterer contains the pressure vector from the scatterer to be nulled, the CSDM is constructed to compute the weighting vector to steer the null. Once the adaptive weighting on the array is computed, the time-reversal mirror can be focused onto the weak target with one iteration. The simulation shows that the focused field in this way gives the identical field to that resulting from the eigenvector with the second largest eigenvalue of the time-reversal operator (TRO) of the DORT method. It is noted that the DORT method requires measurement of the $(N\times N)$ interelement response matrix, while the selective focusing method based on nulling process needs only a few iterations depending on the relative strength of the targets. Typically the number of iteration requires less than the number of array elements. For two targets with target strengths differing by 6 dB, it has been found that ten iterations in total were sufficient to focus on the weaker target.

The potential application of null steering can be found in many areas, including selective focusing, silencing certain locations during transmission and communication associated with TRM, suppressing reverberation from discrete scatterers, and the practical problems that require manipulation of the field based on nulling.

In Sec. II, the formulation of TRM is reviewed and extended to accommodate adaptively weighted backpropagation. Simulation results are presented in Secs. III and IV for null steering and selective focusing, respectively.

II. THEORY

A. Review of TRM

As described in Fig. 1, the phase-conjugate field at the field location $\vec{r}$ in frequency domain is written as[10]

$$p(\vec{r})=\sum_{i=1}^{N} g^*(\vec{r}_i|\vec{r}_{ps})g(\vec{r}|\vec{r}_i)=\mathbf{g}^\dagger(\mathbf{r}_{\text{array}}|\vec{r}_{ps})\mathbf{g}(\vec{r}|\mathbf{r}_{\text{array}}), \quad (1)$$

where $g(\vec{r}_i|\vec{r}_{ps})$ represents the received acoustic pressure at the ith array element location $\vec{r}_i$ propagated from the probe source position $\vec{r}_{ps}$. Likewise, $g(\vec{r}|\vec{r}_i)$ represents the field propagated from the ith array element location $\vec{r}_i$ to the arbitrary receiver location $\vec{r}$ as shown in Fig. 1. N is the number of array elements. Superscripts $(\,)^*$ and $(\,)^\dagger$ denote complex conjugate and Hermitian transpose, respectively. In a vector notation, $\mathbf{g}$ and $\mathbf{r}_{\text{array}}$ are $(N\times 1)$ column vectors. Note that the position vectors are written in *italic* letters with arrows and the column vectors and matrices are written in boldface letters.

[a]The work was done during the author's sabbatical leave at MPL. Permanent affiliation: Korea Maritime University, Pusan, 606-701, Korea. Electronic mail: jskim@hanara.kmaritime.ac.kr

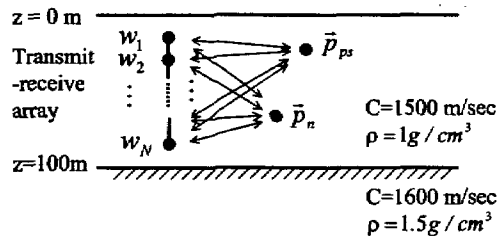

FIG. 1. Description of Pekeris waveguide.

B. Derivation of weight vector

Introducing a signal vector for backpropagation

$$\mathbf{w}=\begin{bmatrix} w_1 \\ w_2 \\ \vdots \\ w_{N-1} \\ w_N \end{bmatrix}, \tag{2}$$

Eq. (1) can, more generally, be written as

$$p(\vec{r})=\sum_{i=1}^{N} w_i^* g(\vec{r}|\vec{r}_i)=\mathbf{w}^\dagger \mathbf{g}(\vec{r}|\mathbf{r}_{\text{array}}), \tag{3}$$

where **w** reduces to **g** in a conventional time-reversal mirror.

Now, let us find a signal vector **w** which gives the distortionless response at the focal point and minimizes the intensity coming from elsewhere when backpropagated. Denoting **K** as the CSDM of the observed signal vector, this problem reduces to the optimization problem of the following objective function:

$$\min_{\mathbf{w}} \mathbf{w}^\dagger \mathbf{K} \mathbf{w}, \tag{4}$$

with the distortionless response constraint at the focal location, which can be expressed as

$$\mathbf{w}^\dagger \mathbf{g}(\vec{r}_{ps}|\mathbf{r}_{\text{array}})=1. \tag{5}$$

The solution is well known and referred to as the minimum variance method in the adaptive array signal processing;[5–7] that is

$$\mathbf{w}=\frac{\mathbf{K}^{-1}\mathbf{g}(\vec{r}_{ps}|\mathbf{r}_{\text{array}})}{\mathbf{g}^\dagger(\vec{r}_{ps}|\mathbf{r}_{\text{array}})\mathbf{K}^{-1}\mathbf{g}(\vec{r}_{ps}|\mathbf{r}_{\text{array}})}. \tag{6}$$

In practice, the signal vector **w** is found from the minimum variance formulation with diagonal loading known as white noise constraint (WNC) in order to make it robust to the noise and the inversion of matrix **K** possible.

For the case of steering a null with a single probe source, the CSDM is defined as

$$\mathbf{K}=\mathbf{g}(\vec{r}_{ps}|\mathbf{r}_{\text{array}})\mathbf{g}^\dagger(\vec{r}_{ps}|\mathbf{r}_{\text{array}})+\mathbf{g}(\vec{r}_n|\mathbf{r}_{\text{array}})\mathbf{g}^\dagger(\vec{r}_n|\mathbf{r}_{\text{array}}), \tag{7}$$

where $\vec{r}_n$ is the location where the null is to be placed. The signal vector **w** in Eq. (6) places a null at the location $\vec{r}_n$ where the Green's function is denoted as $\mathbf{g}=\mathbf{g}(\vec{r}_n|\mathbf{r}_{\text{array}})$. The properties of the signal vector **w** give the distortionless response in the look location when backpropagated, which is expressed as a constraint given in Eq. (5). In addition, since

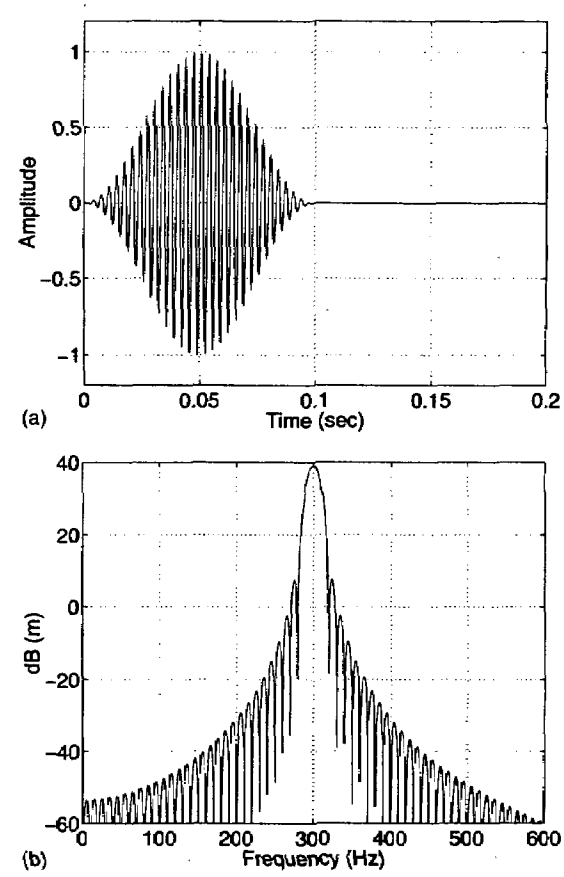

FIG. 2. Probe source (a) signal and (b) spectrum.

the weighting minimizes the acoustic intensity coming from elsewhere, the weighting tends to null out the contributions from other CSDMs such as the second term in Eq. (7), which satisfy the following requirement:

$$\min_{\mathbf{w}} |\mathbf{w}^\dagger \mathbf{g}(\vec{r}_n|\mathbf{r}_{\text{array}})|^2. \tag{8}$$

If the placement of nulls is needed at more than one location, additional CSDMs which correspond to the desired null locations can be added incoherently to Eq. (7).

C. Theory on the waveguide invariants

As described above, the adaptive weight vector normally requires measurement of CSDM for the nulling location. The CSDM, however, can be predicted in an acoustic waveguide if the null is to be placed in the vicinity of the probe source in the range direction using the waveguide invariants theory.

In a dispersive and multimodal waveguide, the lines of constant sound intensity lead to a constant slope between the certain parameters of the waveguide.[8–11] The invariant, denoted as β, characterizes the relation between the range and frequency as

$$\beta=\frac{R}{\omega}\frac{\delta\omega}{\delta R}, \tag{9}$$

where R is a horizontal range and ω is an angular frequency.

For a Pekeris waveguide, β is one as shown in Fig. 9 so that

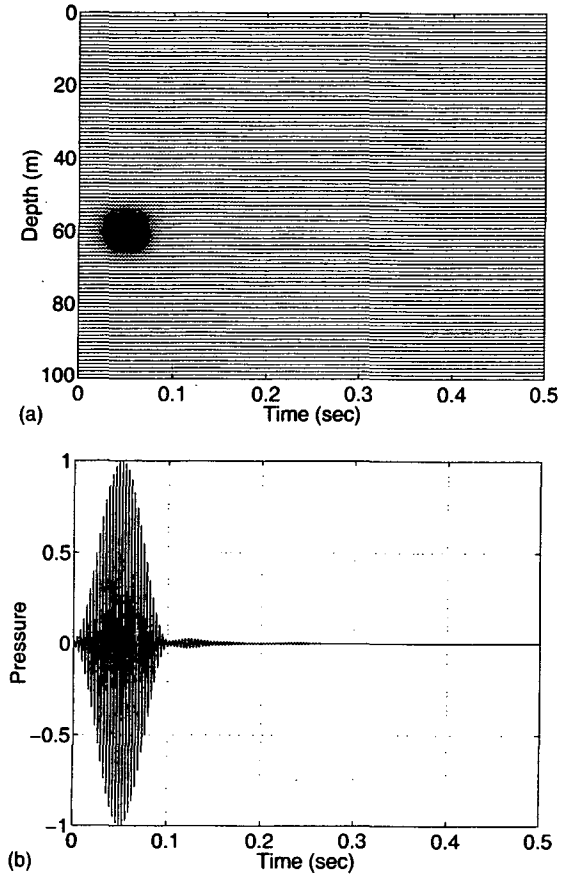

FIG. 3. Simulated time series focused on the probe source location at 60-m depth and 6000-m range.

$$R' = \frac{\omega'}{\omega} R. \tag{10}$$

Equation (10) states that the acoustic field at (R',ω) approximates the value at (R,ω'). Therefore, the signal vector received at the array can be used to calculate the CSDM in the vicinity of the probe source range at the same depth so as to place a null without measuring the Green's function from the null location.

III. SIMULATION IN WAVEGUIDE

In this section, the steering of null is demonstrated in a Pekeris waveguide as shown in Fig. 1. A time-reversal mirror is used to focus on the probe source location in Sec. III A. In Sec. III B, the null is steered to the location of which the transfer function to the array is known. In Sec. III C, the null is steered into the horizontal direction using the transfer function predicted from the theory on the waveguide invariants reviewed in Sec. II C.

For the purpose of simulation, the pulse with center frequency $f_c = 300$ Hz and ping duration $\tau = 0.1$ s is used (Fig. 2). The sampling frequency is 3600 Hz, FFT size is 8192, so that the time window is 2.3 s long. The probe source is located at $\vec{r}_{ps} = (r_{ps}, z_{ps}) = (6000\text{ m}, 60\text{ m})$.

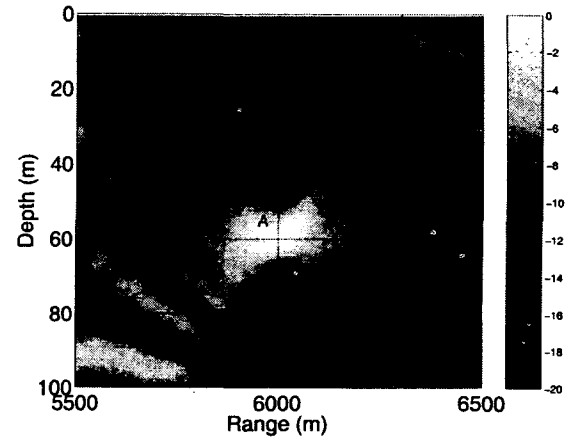

FIG. 4. Single frequency phase conjugation experiment at 300 Hz. The probe source is at 60-m depth and 6000-m range.

A. Time-reversal mirror

When the received signal at the array is time reversed and backpropagated, the signal focuses back to the probe source location as shown in Fig. 3. Figure 3(a) shows the time series received at the range 6000 m as function of depths. The time is referenced as the source signal for the focused signal, since the field response is 1 at the focal point. The focusing is noted at 60-m depth, the time series of which is shown in Fig. 3(b).

Figure 4 shows the focusing at the center frequency 300 Hz. The position A: $\vec{r}_{ps} = (r_{ps}, z_{ps}) = (6000\text{ m}, 60\text{ m})$ is the focal location, B: $\vec{r}_n = (r_n, z_n) = (6300\text{ m}, 80\text{ m})$ is the location to be nulled in Sec. III B, and C: $\vec{r}_n = (r_n, z_n) = (6300\text{ m}, 60\text{ m})$ is the location to be nulled in Sec. III C.

B. Placing a null at an arbitrary location with known field response

When the pressure vector or Green's function at the nulling position $\vec{r}_n = (r_n, z_n)$ from an array is known, the CSDMs are constructed using Eq. (7) and the weight vector is found from Eq. (6). The backpropagated field response with this weighting is shown in Fig. 5 for the center fre-

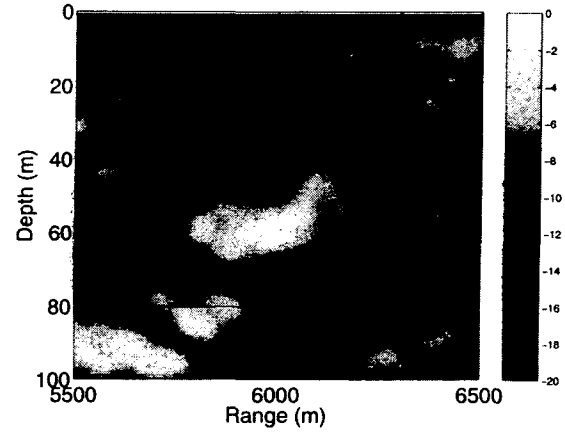

FIG. 5. Single frequency phase conjugation experiment at 300 Hz. The probe source is at 60-m depth and 6000-m range, and a null is placed at the range of 6300 m and at the depth of 80 m.

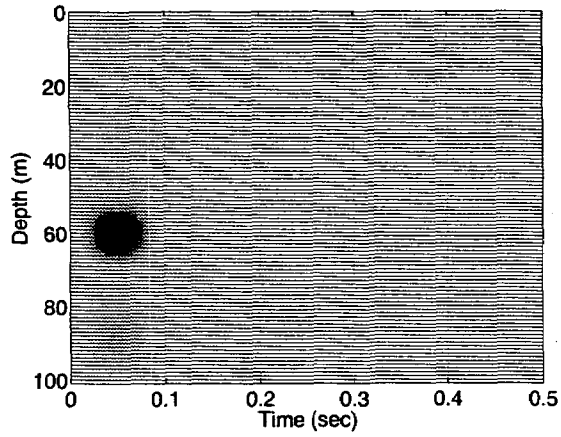

FIG. 6. Simulated backpropagated time series at range 6000 m with a null at 80-m depth and 6300-m range.

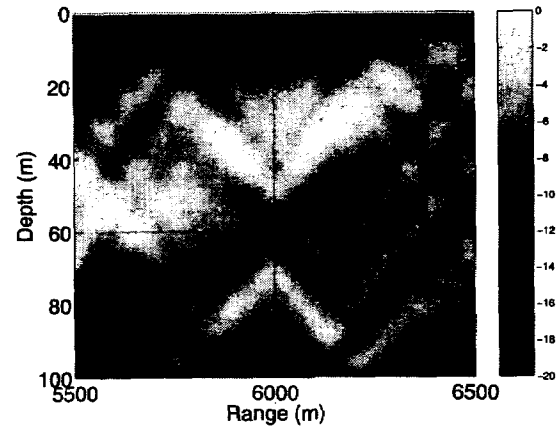

FIG. 8. Single frequency phase conjugation experiment at 300 Hz. The null is steered to the probe source location at the range of 6000 m and at the depth of 60 m.

quency of the probe source signal. The null at point B $\vec{r}_n = (r_n, z_n)$ is noted as a result of the nulling process.

The time series at the range of 6000 m is shown in Fig. 6. Although the distortionless response at the focal location $\vec{r}_{ps} = (r_{ps}, z_{ps})$ is maintained, the weak sidelobes are observed at different depths. This is due to the shading effect of nulling, so that the field except the focal location at the range of 6000 m is modified to some extent. The degree of modification becomes insignificant when the pressure vectors from the probe source location and the nulling location are well resolved. In Fig. 7, the nulling at 80-m depth is shown. The sidelobe structure along the depth at the range of 6300 m is highly correlated with the sidelobe structure in Fig. 5 for the center frequency. Also, the time delay of 0.2 s due to the distance of 300 m from the focal location is noted.

In Fig. 8, a null is steered to the probe source location. A unit vector was used to construct the first term in Eq. (7), which is equivalent to steering the look location to the plane wave propagating normal to the array. The second term in Eq. (7) is now the signal vector from the probe source. This example demonstrates that null can be steered even without the specific look location as a probe source.

C. Placing a null and a focus at the same depth using information from probe source signal only

In Sec. III B, *a priori* knowledge of the pressure vector at the nulling location is required to steer the null. However, even if the pressure vector at the array from the nulling location is not known and the pressure vector from the probe source is the only information available, it is possible to steer the null at the same depth of the probe source within the range where the invariants of waveguide hold.

The transfer function at the null position is predicted based on the theory on the waveguide invariants as described in Sec. II C. Since the null is to be placed at the range of 6300 m, the frequency of the wave vector to be backpropagated in place of 300 Hz can be calculated from Eq. (10) as

$$f' = 300 \text{ Hz} \times \frac{6000 \text{ m}}{6300 \text{ m}} = 285.7 \text{ Hz}. \tag{11}$$

Similarly, the frequency bins are shifted according to Eq. (9), phase conjugated, and backpropagated to realize the null at 6300 m. The null position can also be predicted from Fig. 9.

In Fig. 10, the simulated field response to place a null at 60-m depth and 6300-m range is shown at the center frequency.

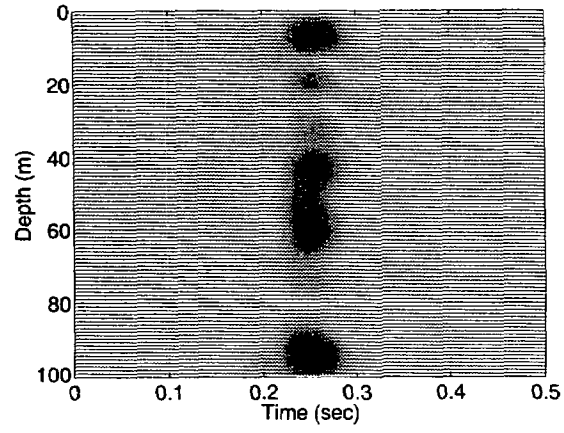

FIG. 7. Simulated backpropagated time series at range 6300 m. Note the null at 80-m depth. Also, 0.2 s of time delay is noted.

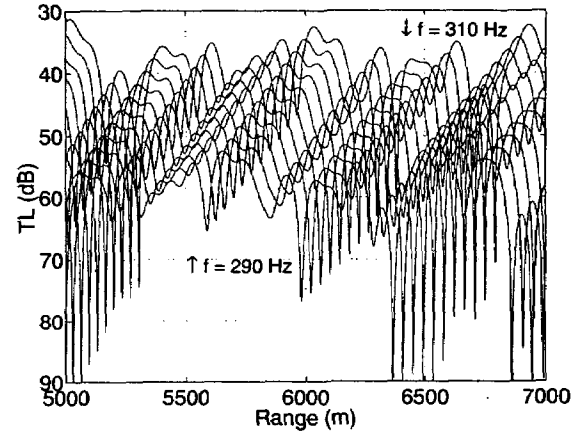

FIG. 9. Interference structure of the sound field in the Pekeris waveguide.

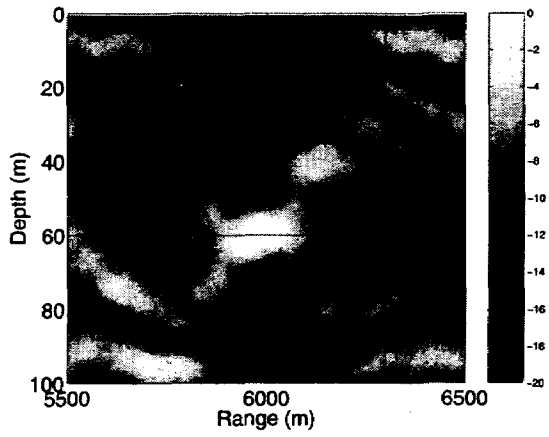

FIG. 10. Single frequency phase conjugation experiment at 300 Hz. The probe source is at 60-m depth and 6000-m range, and a null is placed at the range of 6300 m and at the depth of 60 m.

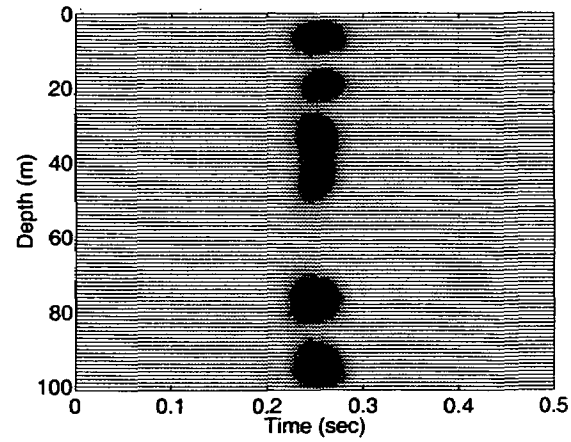

FIG. 12. Simulated backpropagated time series at range 6300 m. Note the null at 60-m depth.

Figure 11 shows the depth-stacked time series at 6000-m range. In Fig. 12, the depth-stacked time series at 6300-m range are displayed. The null at 60-m depth and time delay of 0.2 s is noted.

IV. SELECTIVE FOCUSING ON TWO TARGETS IN FREE SPACE

As an application of null steering, selective focusing associated with the iterative TRM is demonstrated in this section.

Selective focusing on the point-like scatterers has been demonstrated using the DORT method.[4,12] The DORT method utilizes the time-reversal operator (TRO) defined as **K*K**, where the matrix **K** is the transfer matrix, of which elements K_{lm} are defined as the pressure received at lth element with source located at mth element in a transmit–receive array. Note that this **K** is different from the one used in Eq. (4). When the eigenvalues of TRO are not degenerate, the eigenvectors of the TRO correspond to the pressure vectors received from the scatterers. The propagation of the eigenvectors results in selective focusing at each scatterer.

The focusing on the weak target based on nulling process requires the knowledge of CSDM at the location of the strong scatterer in order to calculate the nulling weight vector. This is achieved by an iterative time-reversal operation.[13–15] The received pressure vector from the strong scatterer provides the CSDM at the nulling location. Once the CSDM is known, the weight is calculated and applied on the array before backpropagation. This beam pattern has a null at the location of the strong target and, since the strong eigenvector is suppressed, the beam pattern focuses weakly on the second target. The scattering at this stage occurs from the second target, since the strong target has been nulled. Time reversing and backpropagating this signal yields a focus on the second target.

While the DORT method provides an elegant way for selective focusing, the construction of TRO requires measurement of the $(N\times N)$ interelement response matrix (or, half due to the symmetry of the **K** matrix) and the eigenvector decomposition. The nulling method requires only a few iterations to focus on the second target for the case of two scatterers.

The selective focusing process based on the nulling method is illustrated in the following subsections. Section IV A describes the setup for the numerical experiment and the simulation parameters. In Sec. IV B, the iterative time-

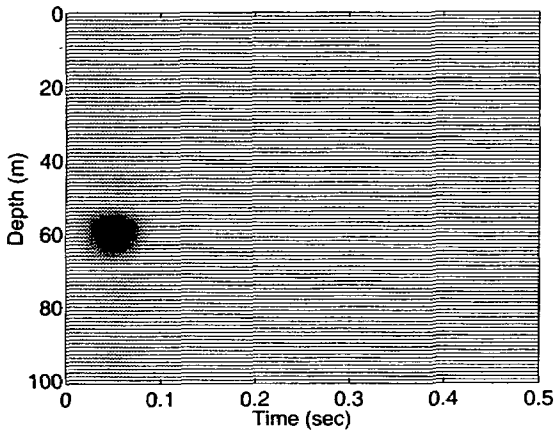

FIG. 11. Simulated backpropagated time series at range 6000 m.

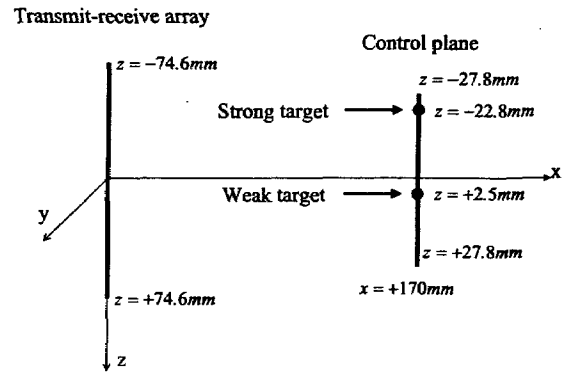

FIG. 13. Setup for numerical experiment of selective focusing.

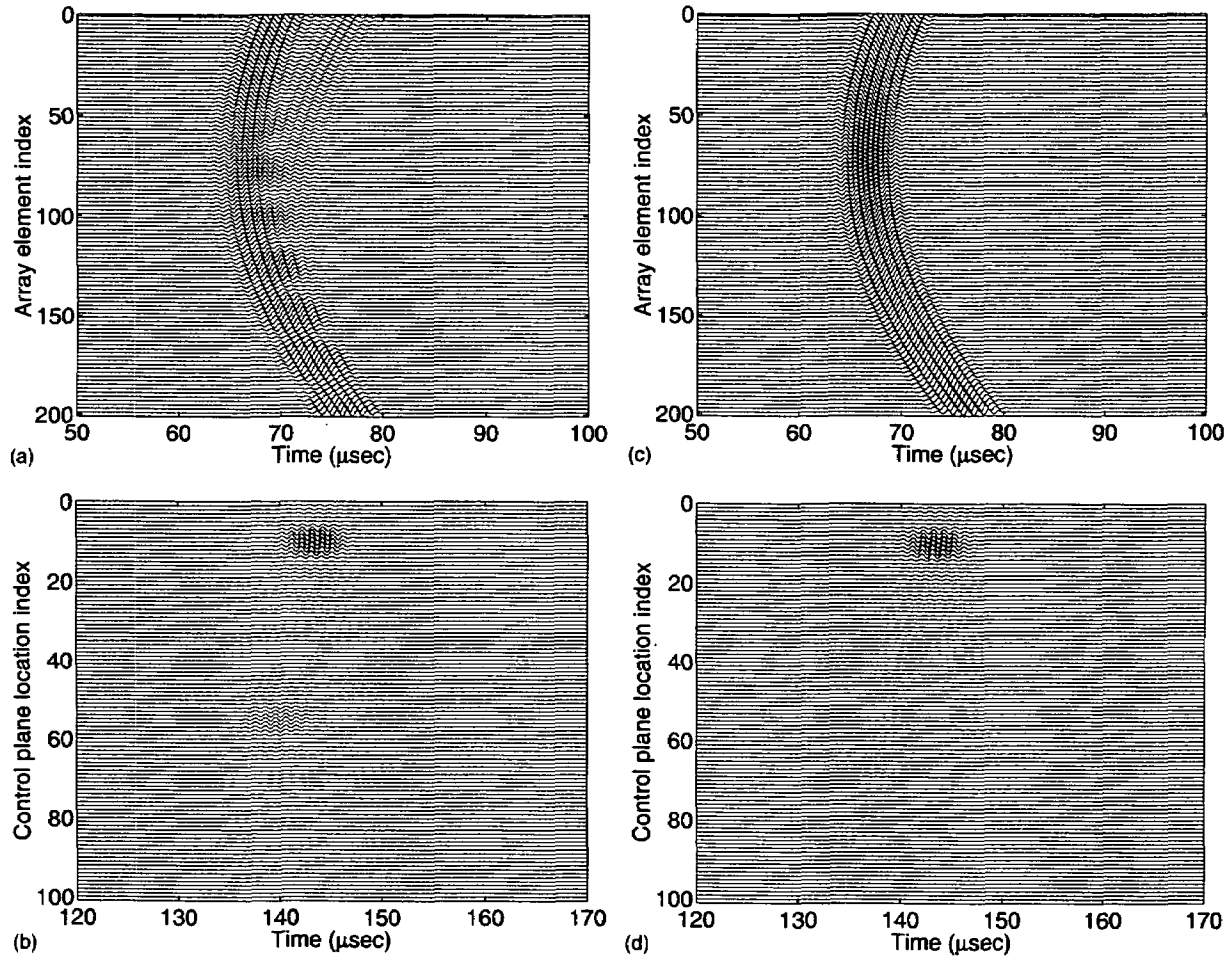

FIG. 14. The time series at the array: (a) and (c), and at the control plane: (b) and (d). (a) Shows the signals received at the array from the scatters insonified by a monopole source. (b) is for the received signals at the control plane when signal (a) is phase conjugated and backpropagated. (c) is the signal received at the array after ten iterations, and (d) is the received signal at the control plane when signal (c) is phase conjugated and backpropagated.

reversal mirror is demonstrated, with selective focusing on the weak scatterer in Sec. IV C.

A. Setup for numerical experiment

Figure 13 shows the schematic setup for the numerical experiment. This setup has been adopted from the experimental setup used in the demonstration of the DORT method[4] with minor modification. The center frequency is 1 MHz, and the sound speed is 1500 m/s. The transmit–receive array has 200 elements with element spacing of half a wavelength, so that z spans between $z=(-74.6,+74.6)$ mm. In order to make the mathematical manipulation more feasible, a control plane (more precisely a line) is defined at 170 mm apart from, and parallel with, the transmit–receive array. The pressure field along this control plane will be displayed to visualize the focusing on the scatterers, which are purposely placed on the control plane. This is not necessary for either the DORT method or the nulling method, since the scatterers can be spread arbitrarily in three-dimensional space. The control plane consists of 100 points. The spacing between the control points are 3/4 of that of the spacing in the transmit–receive array, so that z spans between $z=(-27.8, +27.8)$ mm. Again, this spacing is selected for the purpose of displaying the focusing with fine resolution. Two point scatterers are placed on the control plane. The strong scatterer is at $(x,y,z)=(170,0,-22.8)$, and the weak scatterer is at $(x,y,z)=(170,0,2.5)$. All units are in mm. The scatterers are separated in a way that the scatterers are well resolved. The difference in the target strength is 6 dB for the current simulation. The numerical experiment has been carried out with −30-dB Gaussian white noise. In the simulation, it is assumed that multiple scattering is negligible.

B. Iterative TRM on strong target

In order to achieve the focusing on the strong scatterer, the first step is to insonify the control plane using a point source. The reflected signals from two point scatterers are shown in Fig. 14(a). This signal shows the considerable reflection from the strong scatterer, while there is a weak signal from the second target. When this signal is time reversed and backpropagated, the signal received at the control plane is shown in Fig. 14(b). This process is iterated to achieve a focus on the strong target. After ten iterations, the signal received at the transmit–receive array is shown in Fig. 14(c), for which the time-reversed and backpropagated signal is shown in 14(d). It is clear that the signal is focused on the

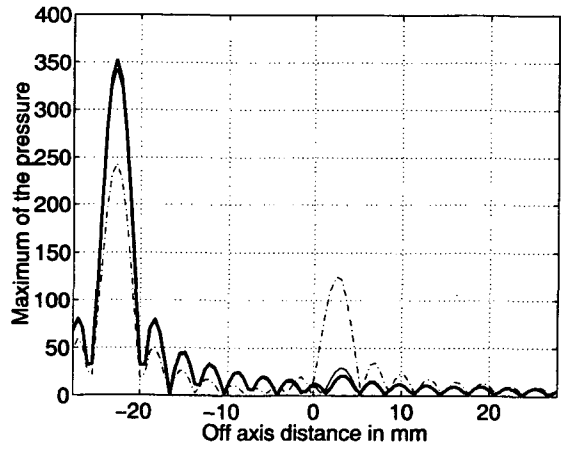

FIG. 15. The field received at the control plane at the center frequency of 1 MHz as the iteration increases. The broken line is the signal received from scatterers insonified by a point source. The amplitude at the strong scatterer is twice that of the weak scatterer. The solid thin line is after five iterations, and the thick line is for the tenth iterations. It shows that the frequency response converges to the strong scatterers.

location of the strong scatterer.

The field projected on the control plane for the center frequency is plotted in Fig. 15. The plot shows how the field is focused to the strong target as the iteration increases. The broken line shows the initial field at the control plane corresponding to the case shown in Fig. 14(b). The difference in the target strengths between scatterers is 6 dB. The thick solid line shows the focusing on the strong target after ten iterations.

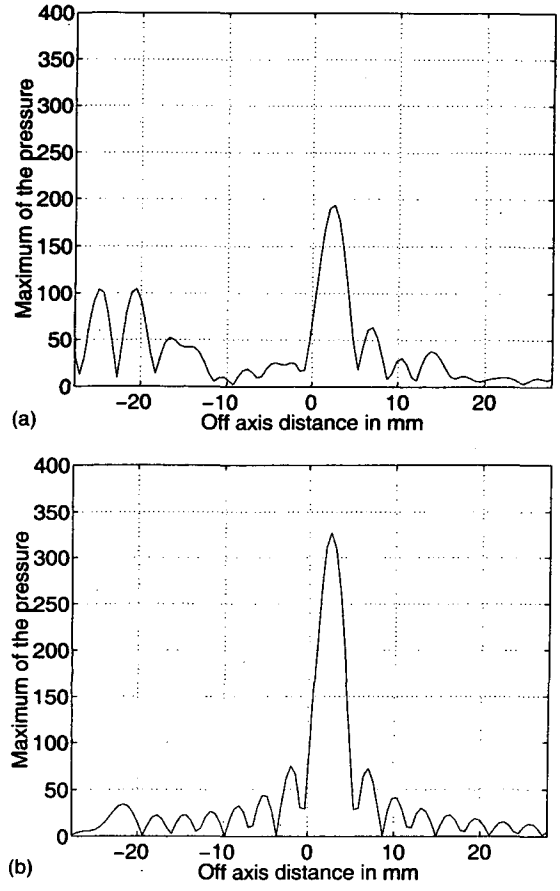

FIG. 16. The wave vectors received at the control plane with nulling. (a) The wave vectors received at the control plane after applying a nulling vector on the phase conjugated transmitting vector at the center frequency. (b) One iteration is applied to focus on the weak target.

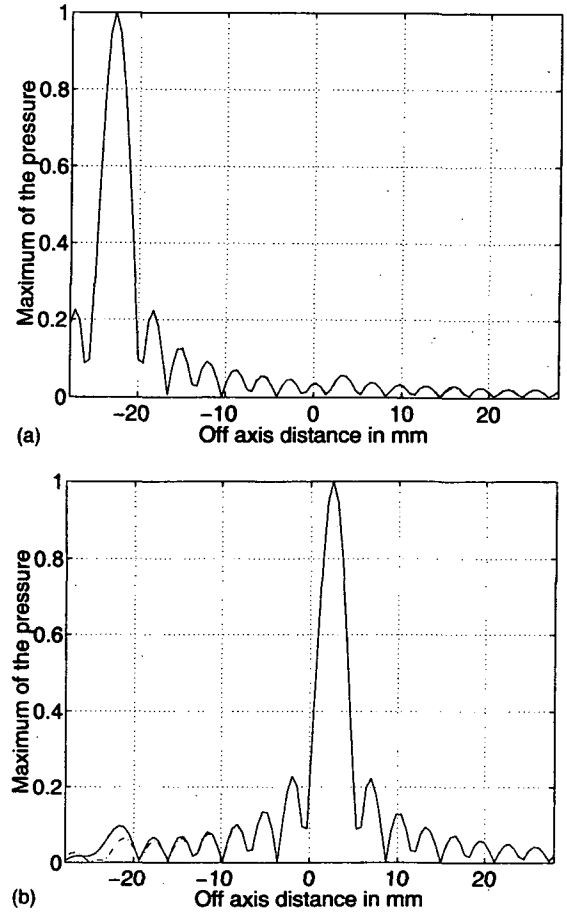

FIG. 17. The comparison with TRO (time-reversal operator). (a) shows the strong scatterer's eigenvectors (broken line: by DORT method; solid line: by iteration). (b) shows the weak scatterer's eigenvectors (broken line: by DORT method; solid line: by nulling method).

The rate of convergence is dependent on the relative target strength of the scatterers. The detailed convergence analysis can be found in Refs. 13–15.

C. Focusing on weak target

Once the focusing on the strong target is accomplished, the signal received at the receive array plays the role of a probe signal where we want to place a null, assuming the scatterer can be treated as a point scatterer. Now, the pressure vector received from the strong target is equivalent to $\mathbf{g}(\mathbf{r}_{\text{array}}|\vec{r}_n)$ in Eq. (7). Note that for this case $\vec{r}_n$ in the second term is the same as $\vec{r}_{ps}$ since the strong scatterer is to be nulled. However, there is the problem of setting the wave vector for which the weighted and backpropagated field has the distortionless response, which plays the same role as the first term in Eq. (7). Although this wave vector can be an arbitrary vector sufficiently far away from the nulling point

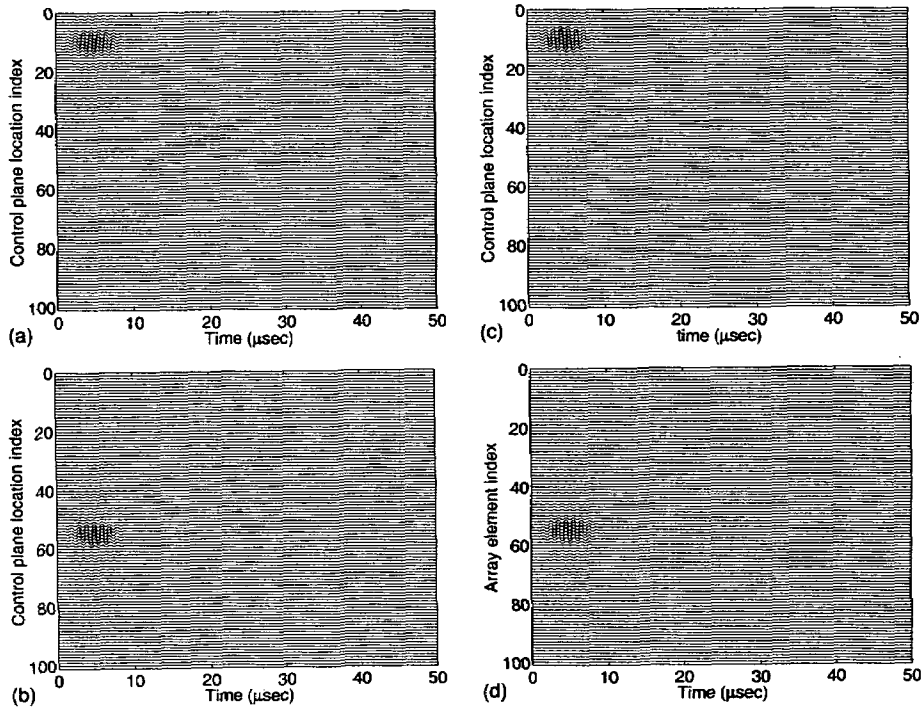

FIG. 18. (a) and (c) show the time series focused on the first target by nulling and DORT methods, respectively, and (b) and (d) show the time series focused on the second target by nulling and DORT method.

(or equivalently well resolved), a unit vector has been used in this study. The meaning of using a unit vector is interpreted as the wave vector received in the far field so that the distortionless response is achieved at the far field. It is noted that the random Gaussian number has been generated to be used as the wave vector for the distortionless response, and the result was unaffected, which is not surprising because the number of elements have enough degrees of freedom to null out the strong eigenvector.

Figure 16(a) shows the pressure vector received at the control plane with the nulling vector applied at the center frequency of 1 MHz. It is noted that considerable focusing is achieved on the weak target. It is considered that, when the strong target eigenvector component is suppressed, the second eigenvector is taking the place of the dominant wave vector. After one iteration, Fig. 16(b) shows that the focusing is achieved on the weak target. If the iteration continues, the strong target will pick up the energy and eventually dominate.

Figures 17(a) and (b) show the focused fields on the strong and the weak targets, respectively, using both the adaptive nulling method and the DORT method. Figure 18 corresponds to the time-domain solution of Fig. 17. Figures 18(a) and (b) show the signal received at the control plane and focused on the strong scatterer located at -22.8 mm, which corresponds to the control panel index of 10, and the weak target located at 2.5 mm, the control panel index of which corresponds to 55. Figures 18(c) and (d) are the same plots using the DORT method. The time delay for the nulling method is arbitrary since there are many iterations involved, while the time delay in the DORT method represents the distance from the transmit–receive array.

V. CONCLUSION

The concept of the weighted time-reversal mirror is introduced. This is used to steer nulls in the Pekeris ocean waveguide to the location where the pressure vector is known at the array while maintaining the distortionless response at the desired location such as a focal point. Using information from the probe source only, the theory on the waveguide invariants is utilized to demonstrate the steering of nulls in the range direction. As an application, selective focusing on the weak target among two point scatterers in free space is realized, giving the identical eigenvectors as obtained from the DORT method.

ACKNOWLEDGMENT

This work was supported by the Office of Naval Research.

[1] M. Fink, "Time-reversal mirrors," J. Phys. D **26**, 1330–1350 (1993).
[2] M. Fink, "Time-reversed acoustics," Phys. Today **50**, 34–40 (1997).
[3] W. A. Kuperman, W. S. Hodgkiss, H. C. Song, T. Akal, C. Ferla, and D. R. Jackson, "Phase conjugation in the ocean: Experimental demonstration of an acoustic time reversal mirror," J. Acoust. Soc. Am. **103**, 25–40 (1998).
[4] C. Prada, S. Manneville, D. Spoliansky, and M. Fink, "Decomposition of the time reversal operator: Detection and selective focusing on two scatterers," J. Acoust. Soc. Am. **99**, 2067–2076 (1996).
[5] Don H. Johnson and Dan E. Dudgeon, *Array Signal Processing—Concepts and Techniques*, Prentice-Hall Signal Processing Series, Alan V. Oppenheim, Series Editor (Prentice Hall, Englewood Cliffs, NJ, 1993).
[6] H. Cox, "Robust adaptive beamforming," IEEE Trans. Acoust., Speech, Signal Process. **ASSP-35**, 1365–1376 (1987).
[7] J. Capon, "High resolution frequency wavenumber spectrum analysis," Proc. IEEE **58**, 1408–1418 (1969).
[8] S. D. Chuprov, "Interference structure of a sound field in a layered

ocean," Acoustics of the Ocean: Current Status (in Russian), edited by L. M. Brekhovskikh and I. B. Andreevoi (Nauka, Moscow, 1982), pp. 71–91.

[9]G. A. Grachev, "Theory of acoustic field invariants in layered waveguide," Acoust. Phys. **39**, 33–35 (1993).

[0]H. C. Song, W. A. Kuperman, W. S. Hodgkiss, T. Akal, and C. Ferla., "A time-reversal mirror with variable range focusing," J. Acoust. Soc. Am. **103**, 3234–3240 (1998).

[1]G. L. D'Spain and W. A. Kuperman, "Application of waveguide invariants to analysis of spectrograms from shallow water environments that vary in range and azimuth," J. Acoust. Soc. Am. **106**, 2454–2468 (1999).

[12]N. Mordant, C. Prada, and M. Fink, "Highly resolved detection and selective focusing in a waveguide using the D.O.R.T. method," J. Acoust. Soc. Am. **105**, 2634–2642 (1999).

[13]C. Prada, F. Wu, and M. Fink, "The iterative time reversal mirror: A solution to self-focusing in the pulse echo mode," J. Acoust. Soc. Am. **90**, 1119–1129 (1991).

[14]C. Prada, J. L. Thomas, and M. Fink, "The iterative time reversal process: Analysis of the convergence," J. Acoust. Soc. Am. **97**, 62–71 (1995).

[15]H. C. Song, W. A. Kuperman, and W. S. Hodgkiss, "Iterative time reversal in the ocean," J. Acoust. Soc. Am. **105**, 3176–3184 (1999).